Lawrence Berkeley National Laboratory
LBL Publications

Title

Thickness dependence of piezo-bimorph adaptive mirror bending

Permalink

https://escholarship.org/uc/item/6r69g4xj

Journal

Review of Scientific Instruments, 94(7)

ISSN

0034-6748

Authors

Goldberg, Kenneth A

La Fleche, Kyle T

Publication Date

2023-07-01

DOI

10.1063/5.0154575

Copyright Information

Peer reviewed

Thickness dependence of piezo-bimorph adaptive mirror bending

Kenneth A. Goldberg ✉ iD ; Kyle T. La Fleche iD

Check for updates

View Online   Export Citation   CrossMark

Articles You May Be Interested In

Theory of magnetic force driven magnetoelectric effect in piezo-bimorph/ferrite cantilever composite

AIP Advances (April 2021)

High-speed adaptive optics using bimorph deformable x-ray mirrors

Rev. Sci. Instrum. (February 2019)

Development of a glue-free bimorph mirror for use in vacuum chambers

Rev. Sci. Instrum. (February 2019)

Thickness dependence of piezo-bimorph adaptive mirror bending

View Online   Export Citation   CrossMark

Kenneth A. Goldberg[1,a] ID and Kyle T. La Fleche[2] ID

AFFILIATIONS

[1] Advanced Light Source Division, Lawrence Berkeley National Laboratory, Berkeley, California 94720, USA
[2] Engineering Division, Lawrence Berkeley National Laboratory, Berkeley, California 94720, USA

[a] Author to whom correspondence should be addressed: KAGoldberg@lbl.gov

ABSTRACT

A new generation of adaptive x-ray optics (AXO) is being installed on high-coherent-flux x-ray beamlines worldwide to correct and control the optical wavefront with sub-nm precision. These ultra-smooth mirrors achieve high reflectivities at glancing angles of incidence and can be hundreds of mm long. One type of adaptive x-ray mirror relies on piezoelectric ceramic strips which are segmented into channels and actuated to induce local, longitudinal bending, generating one-dimensional shape changes in the mirror substrate. A recently described mirror model uses a three-layer geometry with parallel actuators on the front and back surfaces of a thicker mirror substrate. By analogy to a solved problem in the thermal actuation of a tri-metal strip, we show that the achievable bending radius varies approximately as the square of the substrate thickness. We provide an analytic solution and simulate bending using a finite-element model.

05 October 2023 16:14:18

I. INTRODUCTION

Advanced optical elements are being developed for x-ray beamlines to meet the demands of new and emerging high-coherent-flux x-ray light sources. In the field of x-ray optics where ultra-smooth mirrors achieve high reflectivity at glancing angles of incidence, adaptive, bendable mirrors are being deployed to correct and control the wave-front shape, enabling these beamline optical systems to reach diffraction-limited quality.[1–7]

Owing to angles of incidence below 2°, typical x-ray mirrors are hundreds of millimeters long, even for mm-scale beam cross-sectional widths. Furthermore, to operate at these short wavelengths, mirrors must be polished—either flat or curved—to nanometer-scale shape and surface tolerances, and the required shapes must be preserved during use. Sensitivity to shape errors on the scale of fractions of a nanometer puts stringent demands on mechanical mounting, beam-induced thermal distortion, and environmental conditions.

For x-ray mirrors, a traditional approach has been to make the mirror substrates thick enough (and thus stiff enough) to preserve the surface shape when mounted. Yet bendable mirrors require a balance between stiffness and flexibility: they must be able to bend to the required local radius values. This study is motivated by the need to understand the relationship between substrate thickness and bending radius.

Silicon is commonly used as the substrate material because it can be polished to nearly atomic-scale precision (sub-nm rms) and has favorable thermal properties (i.e., relatively high conductivity). Adaptive x-ray mirrors are commonly shaped as rectangular prism substrates and may be coated with a thin metal layer or multilayer to enhance reflectivity.

The creation and use of adaptive x-ray mirrors with piezo-bimorph actuation has been an active area of research since the 1990s. Sutter *et al.* presented a history of developments and progress in this field through 2022.[8] Briefly, at the European Synchrotron Radiation Facility (France), Susini *et al.*[9,10] and later Signorato *et al.*[11] created a geometry with a piezo-bimorph sandwiched between mirror substrates. These early experiments and analyses presaged many of the primary issues and coming advances. Commercialization by Thales-SESO led to advances that overcame surface shape errors related to the buried junctions. In this second generation, piezoelectric elements are bonded to the side faces of a monolithic substrate. Promising results led to adoption at several facilities, and in the years that followed, there have been continual improvements in lifetime, performance, and dynamic control.[12]

One class of adaptive mirrors recently described by Ichii *et al.* has piezoelectric ceramic material bonded symmetrically to the front and back surfaces of the mirror substrate, forming a tri-layer geometry with an open central channel.[4] The piezoelectric strips are segmented longitudinally into channels and wired with thin-film electrodes for actuation. The substrate has a uniform rectangular cross section. The front- and back-layer material expands or contracts longitudinally when a voltage differential is applied to the actuators. The strongest bending occurs when opposing voltages are applied to the front and back. When the Si substrate is 10 mm thick, and ±500 V is applied to the two layers, a local bending radius of curvature of ~1 km can be achieved.[4] We find that 1 km is a good target range for local bending radii that will be required in our applications at the Advanced Light Source. Dynamic control and stabilization of a mirror with this form factor have been demonstrated by Gunjala *et al.*[13]

II. MODELING THE ADAPTIVE MIRROR

A tri-layer model of a section of an adaptive mirror with four piezoelectric strips is shown in Fig. 1(a). The model represents a uniform segment of the mirror's length. A symmetric geometry, with identical actuators on the back side, enables the mirror to resist thermal deformation arising from the differing coefficients of thermal expansion between the two materials. The substrate thickness is t_2. The piezoelectric layer thicknesses are t_1 and t_3, respectively, and we take $t_3 = t_1$. Thus, the total system thickness h is $2t_1 + t_2$. The substrate width is b_2. In practice, the piezoelectric actuators do not span the full width of the front surface, allowing an open channel of width w—a clear aperture for the x-ray beam. To study the one-dimensional bending of the structure, the equivalent width of the piezoelectric material b_1 is $b_2 - w$, and we have $b_3 = b_1$ for the bottom layer. A simplified version is shown in Fig. 1(b).

In our analysis, we assume ideal welding or bonding between the layers and a negligible interface thickness.

A well-known result from classical, Euler–Bernoulli beam theory is that the bending radius of curvature varies with t^3. This result applies to a beam of uniform, rectangular cross section with thickness t, simply supported by ends that are allowed to rotate freely and move without friction when the beam is subjected to a uniformly applied force.[14] The t^3 dependence also emerges when bending moments are applied to the ends and the center is unsupported.[1]
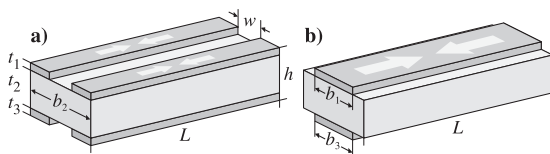
FIG. 1. Models of a tri-layer piezo-bimorph adaptive mirror. The piezoelectric layers are on the front and back sides of a silicon mirror substrate (i.e., top and bottom). (a) The real mirror features an open channel on the front surface for the x-ray beam and symmetric actuators on the back. (b) An equivalent, simplified structure is used for the analytical solution. The model represents a uniform segment of the mirror length where bending forces are applied.

Analysis by Susini *et al.* on the first-generation piezo-bimorph mirror system showed an expected, approximate, t^2 dependence of the bending radius.[9]

Our study's geometry is different: we have a three-layer structure, and the piezoelectric actuators induce shear stress on the front and back surfaces as they expand or contract in the direction parallel to the optical face, not perpendicular to it. Thus, the analysis requires a different approach.

The following sections describe ideal analytical models and the predicted behavior of realistic mirror geometries with finite-element modeling.

III. ANALYTIC MODELING

We model this structure by analogy to the 1925 work of Timoshenko,[15] who studied the beam-bending that arises from differential thermal expansion in a bi-metal (two-layer) strip, and Vasudevan and Johnson,[16] who expanded the analysis to a tri-metal (three-layer) system. Tibi *et al.*[17] is also a helpful reference on this topic. In those studies, bending is driven by the thermal strain at the interfaces, arising from a difference in the thermal expansion coefficients, and the applied temperature change: $(\alpha_1 - \alpha_2)\Delta T$.

Here, following Conrad *et al.*,[18] we substitute thermal strain with piezoelectric strain, which, by design, occurs in a direction perpendicular to the applied voltage, in the long direction of the mirror. This strain is proportional to the coefficient of the piezoelectric tensor, d_{31}, and the applied electric field, E_z: $d_{31}E_z$.[19] The electric field in the layer is given by the applied voltage U and thickness t, as $E = U/t$. (Note that the subscripts of d are related to the crystal axes not to the layers of our system.)

The effects we model represent relatively small shape perturbations, for which a one-dimensional analytical treatment of the local bending radius is a sufficient approximation. In cases of interest for x-ray optics, the bending radii (kilometers) are more than 10 000 times larger than the mirror thickness (millimeters). In addition, we impose the following assumptions. (1) We treat the layers as beams capable of axial bending. (2) The beams bend about a single axis. (3) The deformation is linear. (4) No slipping occurs at the interfaces. (5) Layers have uniform material properties. (6) The applied electric field is uniform within the piezoelectric layers. (7) One edge of the substrate can rotate about its axis (one degree of freedom). (8) The opposite edge can rotate about its axis and translate along the length of the mirror.

In Timoshenko's and Vasudevan's derivations, the strip is taken to have unit width. Here, we reintroduce the width into the expressions to accommodate the different layer widths in our model.

The simplified system geometry is shown in Fig. 2. All of the forces acting over this section of the three layers $\{j\}$ can be represented by axial tensile, compressive forces P_j, and bending moments M_j. Since there are no external forces acting on the system, equilibrium requires[16]

$$P_1 + P_2 + P_3 = 0. \tag{1}$$

The flexural rigidity of the jth layer is E_jI_j. Here, I_j is one layer's moment of inertia or the second moment of the area, defined as $I_j = b_jt_j^3/12$,[14] as shown in Fig. 2. While E_j is Young's modulus, it should not be confused with the applied electric field.
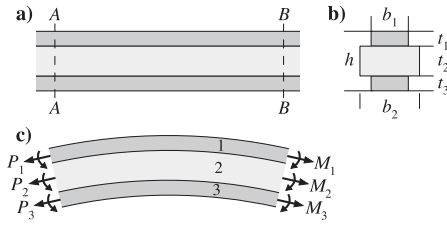
FIG. 2. Simplified geometry of the tri-layer model. The beam is shown (a) from the side and (b) in cross section. With forces (P) and bending moments (M) applied, a bent segment of the beam is shown in (c).

Following Vasudevan, equilibrium requires

$$M_1 + M_2 + M_3 - \frac{P_1 t_1}{2} - P_2\left(t_1 + \frac{t_2}{2}\right) - P_3\left(t_1 + t_2 + \frac{t_3}{2}\right) = 0. \quad (2)$$

Since the bending radius (kilometers) is so much larger than the total thickness of the system (tens of millimeters), we approximate the bending radius of curvature ρ, as the same for all layers. The bending moments for each layer and for the system are, thus,

$$\frac{1}{\rho} = \frac{M_1}{E_1 I_1} = \frac{M_2}{E_2 I_2} = \frac{M_3}{E_3 I_3} = \frac{\Sigma M}{\Sigma EI}, \quad (3)$$

with summations over j.

From these expressions and the equality of intersurface strains at each interface, the general, three-layer equation that Vasudevan derived for the radius of curvature under thermal expansion is

$$\frac{1}{\rho} = \frac{2\Delta T\left[\frac{(\alpha_1-\alpha_2)(t_1+t_2)}{S_3} + \frac{(\alpha_2-\alpha_3)(t_2+t_3)}{S_1} + \frac{(\alpha_1-\alpha_3)(t_1+2t_2+t_3)}{S_2}\right]}{\frac{(t_1+t_2)^2}{S_3} + \frac{(t_2+t_3)^2}{S_1} + \frac{(t_1+2t_2+t_3)^2}{S_2} + \frac{4\,\Sigma EI\,\Sigma S}{S_1 S_2 S_3}}. \quad (4)$$

Consistent with Timoshenko's derivation, Vasudevan's S_j is defined as $t_j E_j$ when the strip has unit width. In order for us to include specific and variable layer widths, S_j becomes $t_j b_j E_j$. (Because Young's modulus has units of pressure, i.e., force per area, the S_j terms have the units of force.)

In our system, layers 1 and 3 have equivalent thickness and material properties. Thus, $t_1 = t_3$, $E_1 = E_3$, $I_1 = I_3$, and $S_1 = S_3$. Allowing for the application of different voltages in the top and bottom layers, the differential thermal expansion terms $(\alpha_i - \alpha_j)\Delta T$ are replaced with $d_{31} U_1/t_1$ and $d_{31} U_3/t_3$ in layers 1 and 3, respectively. Since the substrate layer has no piezoelectric properties, we set the corresponding layer-2 expansion terms to zero.

With these substitutions to the approach of Eq. (4), our piezo-actuated model reduces to a general form with arbitrary voltages applied to the front and back piezoelectric elements,

$$\frac{1}{\rho} = \frac{(t_1 + t_2)d_{31}(U_1 - U_3)}{t_1(t_1 + t_2)^2 + \frac{1}{6}\left(2t_1^3 + \frac{E_2 b_2}{E_1 b_1}t_2^3\right)}. \quad (5)$$

As we expect, the local curvature varies linearly with the applied voltages and the coefficient of the piezoelectric tensor.

Using Eq. (5), we can study several special cases of interest. We observe that the application of equal and opposite voltages,

$U_3 = -U_1$, will halve the local bending radius (doubling the curvature). This is a common way that these mirrors are designed to be used. Equation (5) becomes

$$\frac{1}{\rho} = \frac{2(t_1 + t_2)d_{31} U_1}{t_1(t_1 + t_2)^2 + \frac{1}{6}\left(2t_1^3 + \frac{E_2 b_2}{E_1 b_1}t_2^3\right)}. \quad (6)$$

This result is compared with finite-element modeling in Sec. V.

When a voltage difference is applied only to the top-surface elements (as in Ref. 4), we take $U_3 = 0$, and the calculated curvature is half of the value in Eq. (6).

The significant thickness difference between the substrate and piezo layers allows us to consider limiting cases, with simplified approximations. When the substrate thickness is larger than the piezo-layer thicknesses, Eq. (5) reaches this approximate general-voltage form dependent only on t_2,

$$\frac{1}{\rho} \to 6\left(\frac{E_1 b_1}{E_2 b_2}\right)\frac{d_{31}(U_1 - U_3)}{t_2^2}. \quad (7)$$

And again, when equal and opposite voltages are applied to the two sides ($U_3 = -U_1$), we have

$$\frac{1}{\rho} \to 12\left(\frac{E_1 b_1}{E_2 b_2}\right)\frac{d_{31} U_1}{t_2^2}. \quad (8)$$

The substrate-thickness-squared dependence of the bending radius becomes apparent in Eqs. (7) and (8).

In the complementary case where the substrate thickness is less than that of the piezoelectric layer, the bending radius approaches

$$\frac{1}{\rho} \to \frac{3}{2}\frac{d_{31} U_1}{t_1^2}, \quad (9)$$

a result derived by Conrad et al.[18] Such a case may arise if the thick mirror substrate were replaced by a thin wafer.

IV. FINITE-ELEMENT MODEL

A finite-element model of the mirror system was developed to test the predictions of the analytic treatment and to design mirrors for our applications. The model's dimensions are similar to those described in recent publications,[4] providing an opportunity for comparison to measured data.

Our model was created in Creo Parametric 8.0[20] and imported into a coupled field static analysis system in Ansys[21] for finite-element analysis (FEA). The model begins with a silicon substrate, 150 mm long by 50 mm wide, with a uniform thickness measuring between 10 and 35 mm. Four piezoelectric elements are bonded symmetrically to the front and back surfaces, as shown in Fig. 3. Each measures 100 mm long by 15 mm wide by 1 mm thick. The pads are symmetrically placed alongside a 12 mm wide clear aperture. The mirror is designed to be illuminated at glancing angles of incidence with a narrow beam that falls along the clear aperture.

To assess the thickness dependence of the mirror bending, the substrate thickness was increased in 5 mm increments from 10 to 35 mm while the forces applied by the piezoelectric elements were held constant.

On the experimental mirror, the piezoelectric elements are segmented lengthwise into an array of channels that can be addressed
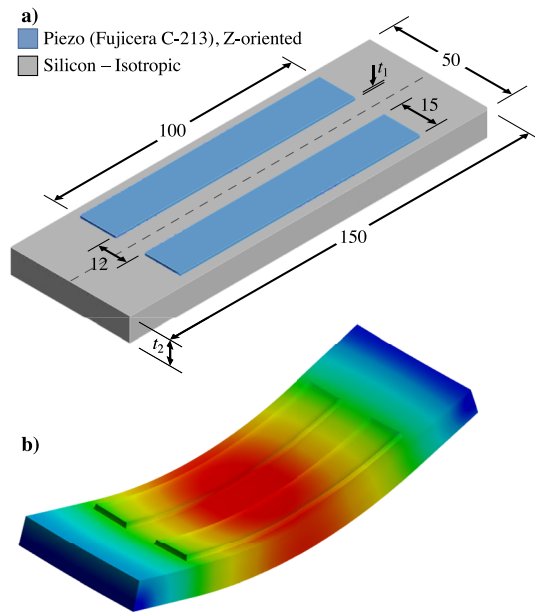
FIG. 3. (a) FEA modeling geometry showing the silicon substrate and the placement of the piezoelectric elements on the top surface. Two, symmetrically-placed piezo elements are also attached to the back side. Surface shape data are extracted along the central meridian (dashed line). All lengths shown are in mm. (b) Exaggerated rendering of the resultant bending from actuation, in one case.

individually. Our model simplifies this configuration, treating the system as four unified, single elements. We provide a voltage differential to the top two elements, U_1, and separately to the back two elements, U_3. With equal and opposite voltages applied to two sides,

TABLE I. Materials properties and dimensions used in this finite-element model.

Property	Value	Reference
Silicon		
Young's modulus, E_2	130 GPa	22
Poisson's ratio, σ	0.28	
PZT[a]		
Young's modulus, Y_{11}^E	82 GPa	23
Young's modulus, Y_{33}^E	66 GPa	
Young's modulus, Y_{55}^E	26 GPa	
Poisson's ratio, σ	0.29	
Piezo charge constant, d_{31}	−135 pm/V	
Piezo charge constant, d_{33}	310 pm/V	
Piezo charge constant, d_{15}	510 pm/V	
Dielectric constant, $\varepsilon_{11}^T/\varepsilon_0$	1590	
Dielectric constant, $\varepsilon_{33}^T/\varepsilon_0$	1470	
Dimensions		
Si mirror size	$150 \times 50 \times t_2$ mm	
PZT size (four elements)	$100 \times 15 \times 1$ mm^3	

[a]PZT—Pb(ZrTi)O$_3$, lead zirconate titanate material C-213.

the resulting forces contract the top-surface actuators and expand the back-surface actuators, creating a one-dimensional concave top face.

Within Ansys, the mechanical–electrical properties of the piezoelectric layers are defined as a custom material. The 6×6 compliance matrix is calculated using elastic and shear moduli provided in the material data sheet for Fujicera C-213 piezoceramic.[23] These values, along with the relative permittivities and piezoelectric charge constants, describe the piezoceramic electro-mechanical behavior. The silicon substrate is treated as a simple, isotropic material. 500 or −500 V is applied to each strip to induce matching expansion and contraction of the back and front of the mirror, respectively.

The model's assumptions and boundary conditions were defined in Sec. III. The material properties are listed in Table I. Note: Regarding the piezo charge constants, m/V is equivalent to C/N.

V. FINITE-ELEMENT ANALYSIS

In the model, the mirror bends in response to the applied forces; the resultant shape is extracted in 202 data points along the central meridian of the front surface (i.e., in the direction of light propagation). The surface deformation (Fig. 4), slope (Fig. 5), and second derivative (Fig. 6) are calculated from the surface profile at each substrate thickness, from 10 to 35 mm. The central radius of curvature (the reciprocal of the second derivative) is shown for each thickness in Fig. 7. The curvature values predicted from Eq. (5) of the analytic model are shown as open circles in Fig. 6 and as a black curve in Fig. 7.

Defining the endpoints of the mirror as zero height, the central sag reaches 6.74 μm when the mirror is 10 mm thick. This shape has a central radius of 367 m. Doubling the substrate thickness to 20 mm, the peak sag is 1.83 μm with a central radius of 1359 m, 3.7 times larger than the 10 mm case.
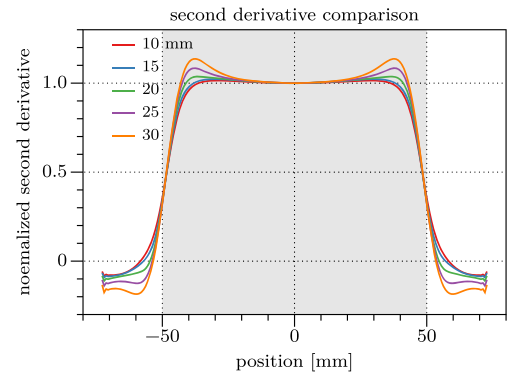
Figures 4 through 7 show the surface deformation, slope, second-derivative, and minimum radius of curvature extracted from the finite-element model. As predicted, the minimum curvature varies approximately with the square of the substrate thickness, t_2.
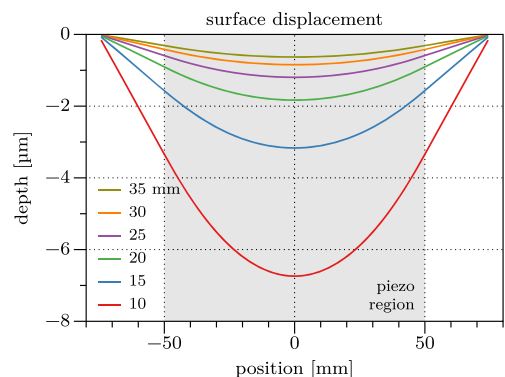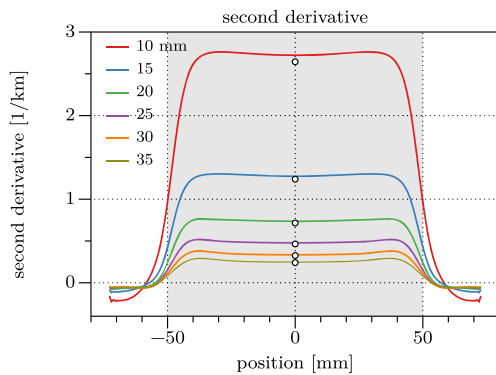

FIG. 4. Calculated mirror surface profiles with varying Si-substrate thickness, t_2, from 10 to 35 mm, but constant voltage. The gray region denotes the length of the mirror over which the piezoelectric materials are attached. In an absolute sense, the micrometer-scale displacements are small compared to the size of the mirror.
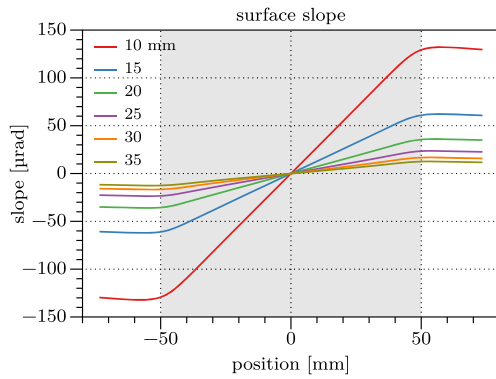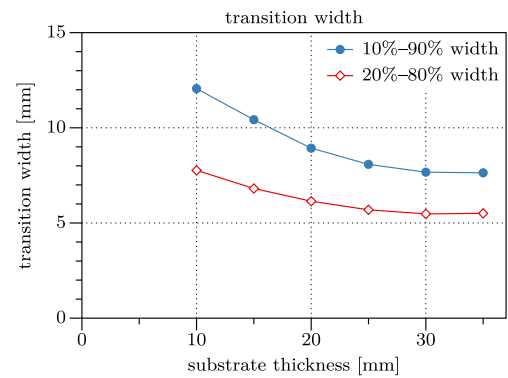
FIG. 5. Slope analysis shows a nearly uniformly varying slope across most of the actively bent region and minimal bending outside of that region. Each curve is one substrate thickness, t_2, as shown.
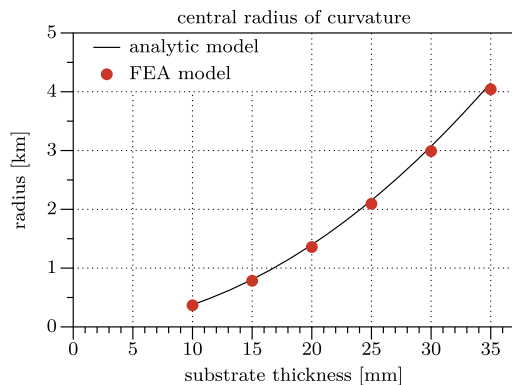

FIG. 6. The second derivative plots show nearly uniform curvatures across the center of the active piezoelectric region and zero values outside. Each curve is one substrate thickness, t_2, as shown. There is a transition region of ~20 mm across that edge. The thinnest substrate bends with the highest curvature. Open circles show the second derivative values predicted from Eq. (6).

FIG. 7. Red circles show the radius of curvature calculated at the center of the mirror for each thickness, t_2. The black curve shows predictions from the analytic model for comparison.

FIG. 8. Comparison of second-derivative curves normalized to the central values.

FIG. 9. The longitudinal transition-region widths at the ends of the piezoelectric material vary as a function of the substrate thickness. The transition widths are measured in two ways, relative to the central values.

The surface contains longitudinal effects that our analytic model (based on a uniform cross-section) does not capture. The shape undergoes a transition across the piezo-element boundaries at ±50 mm. Thickness-dependent boundary widths are apparent in Fig. 8 with the second-derivative curves normalized to their central values. Width values calculated from the curves in Fig. 8 are shown in Fig. 9. Thinner substrates have wider transition regions. This has implications for the spatial range over which individual piezo elements influence the local curvature and for the amount of coupling between adjacent actuators.

VI. CONCLUSION

By providing nanometer-scale optical wave-front correction, adaptive x-ray mirrors will play a central role in the preservation of coherent beam properties on x-ray beamlines and telescopes now and into the future. The balance between stiffness and flexibility requirements is central to the design of these adaptive x-ray mirrors. Realizing new designs requires that we can predict their physical properties and dependencies.

Calculating the bending of beams under external forces is well-known in mechanical engineering textbooks. Yet, unlike the t^3

05 October 2023 16:14:18

thickness dependence of the bending radius that occurs when a beam is placed under uniform perpendicular loads, we find that tri-layer, sandwich-like piezoelectric actuation, with tensile and compressive stresses applied parallel to a mirror's surface, shows an approximate t^2 dependence. We derived this result analytically, following the work of Timoshenko and Vasudevan, and by making the analogy between piezoelectric forces and thermal expansion, as Conrad has shown. We used finite-element modeling to substantiate the results of predictions made with the analytic approach and to observe the behavior at the interfaces. This approximate, thickness-squared dependence we find is qualitatively consistent with previous analysis of first-generation adaptive x-ray mirrors in a different but related system geometry.

AUTHOR DECLARATIONS

Conflict of Interest

The authors have no conflicts to disclose.

Author Contributions

Kenneth A. Goldberg: Conceptualization (lead); Data curation (equal); Formal analysis (equal); Funding acquisition (lead); Investigation (equal); Methodology (equal); Project administration (lead); Resources (lead); Software (equal); Supervision (lead); Validation (lead); Visualization (lead); Writing – original draft (lead); Writing – review & editing (equal). **Kyle T. La Fleche**: Conceptualization (supporting); Data curation (equal); Formal analysis (equal); Investigation (equal); Methodology (equal); Software (equal); Validation (supporting); Visualization (supporting); Writing – original draft (supporting); Writing – review & editing (equal).

DATA AVAILABILITY

The data that support the findings of this study are available from the corresponding author upon reasonable request.

REFERENCES

[1] M. R. Howells, D. Cambie, S. C. Irick, A. A. MacDowell, H. A. Padmore, T. R. Renner, S. Y. Rah, and R. Sandler, Opt. Eng. **39**, 2748 (2000).

[2] K. J. S. Sawhney, S. G. Alcock, and R. Signorato, Proc. SPIE **7803**, 780303 (2010).

[3] D. J. Merthe, K. A. Goldberg, V. V. Yashchuk, W. R. McKinney, R. Celestre, I. Mochi, J. Macdougall, G. Y. Morrison, S. B. Rekawa, E. Anderson, B. V. Smith, E. E. Domning, and H. Padmore, Nucl. Instrum. Methods Phys. Res., Sect. A **710**, 82 (2013).

[4] Y. Ichii, H. Okada, H. Nakamori, A. Ueda, H. Yamaguchi, S. Matsuyama, and K. Yamauchi, Rev. Sci. Instrum. **90**, 021702 (2019).

[5] H. Jiang, N. Tian, D. Liang, G. Du, and S. Yan, J. Synchrotron Radiat. **26**, 729 (2019).

[6] S. G. Alcock, I.-T. Nistea, V. G. Badami, R. Signorato, and K. Sawhney, Rev. Sci. Instrum. **90**, 021712 (2019).

[7] C. Colldelram, N. González, J. González, C. Ruget, J. Juanhuix, and J. Nicolas, AIP Conf. Proc. **2054**, 060013 (2019).

[8] J. P. Sutter, S. G. Alcock, I.-T. Nistea, H. Wang, and K. Sawhney, Synchrotron Radiat. News **35**, 8 (2022).

[9] J. Susini, D. Labergerie, and L. Zhang, Rev. Sci. Instrum. **66**, 2229 (1995).

[10] J. Susini, D. R. Labergerie, and O. Hignette, Proc. SPIE **2856**, 130 (1996).

[11] R. Signorato, O. Hignette, and J. Goulon, J. Synchrotron Radiat. **5**, 797 (1998).

[12] S. G. Alcock, I.-T. Nistea, V. G. Badami, R. Signorato, M. Fusco, L. Hu, H. Wang, and K. Sawhney, Optica **10**, 172 (2023).

[13] G. Gunjala, A. Wojdyla, K. A. Goldberg, Z. Qiao, X. Shi, L. Assoufid, and L. Waller, J. Synchrotron Radiat. **30**, 57 (2023).

[14] W. C. Young and R. G. Budynas, *Roark's Formulas for Stress and Strain*, 7th ed. (McGraw-Hill, New York, 2002), Sec. 8.1, pp. 125–127.

[15] S. Timoshenko, J. Opt. Soc. Am. **11**, 233 (1925).

[16] M. Vasudevan and W. Johnson, J. R. Aeronaut. Soc. **65**, 507 (1961).

[17] G. Tibi, E. Sachyani Keneth, M. Layani, S. Magdassi, and A. Degani, Soft Rob. **7**, 649 (2020).

[18] H. Conrad, T. Klose, T. Sander, H. Schenk, and H. Lakner, *Actuating Methods of Quasistatic Micromirrors for Active Focus variation," 2008 International Students and Young Scientists Workshop - Photonics and Microsystems, Wroclaw-Szklarska Poreba* (IEEE, Poland, 2008), pp. 7–11.

[19] E. Steinhaus and S. G. Lipson, J. Opt. Soc. Am. **69**, 478 (1979).

[20] PTC, Creo Parametric 8.0.2.0, 2021.

[21] Ansys, Ansys Workbench 2022 R2, 2022.

[22] M. A. Hopcroft, W. D. Nix, and T. W. Kenny, J. Microelectromech. Syst. **19**, 229–238 (2010).

[23] The material characteristics of piezoceramics, https://www.fujicera.co.jp/wpkanri/wp-content/uploads/2022/02/39e06c49b38428b2e03aff56b584a225.pdf, 2022; accessed November 15, 2022.

05 October 2023 16:14:18